Chimica Techno Acta
published by Ural Federal University
eISSN 2411-1414; chimicatechnoacta.ru

ARTICLE
2021, vol. 8(2), № 20218211
DOI: 10.15826/chimtech.2021.8.2.11

Structural changes in V_2O_5-P_2O_5 glasses: non-constant force field molecular dynamics and IR spectroscopy

A.A. Raskovalov[a,*], N.S. Saetova[b], I.S. Popov[c]

a: Institute of High Temperature Electrochemistry of UB RAS, 620137 Akademicheskaya st., 20, Yekaterinburg, Russia
b: Vyatka State University, 610000, Moskovskaya st., 36, Kirov, Russia
c: Institute of Solid State Chemistry of UB RAS, 620049 Pervomayskaya st., 91, Yekaterinburg, Russia
* Corresponding author: other@e1.ru

This article belongs to the regular issue.

Abstract

Quasi-binary phosphate-vanadate glasses have been studied by both IR spectroscopy and a novel method of molecular dynamics with a non-constant force field. This method is used for the self-assembly of structural models of glasses. The obtained models and the glass network structure are analyzed quantitatively using element distribution by the number of R–O–R bonds (R is phosphorous or vanadium) and 4-, 6-, and 8-membered cycles. The bends on the concentration dependences of atoms distribution in the second coordination sphere agree well with changing the shape of IR spectra. Based on the cycle analysis, the formation of cycles is shown to be more characteristic for vanadate fragments that can form 4-membered cycles, which, according to Zachariasen's rule, negatively affects glass-forming ability.

Keywords

phosphate-vanadate glasses
IR spectroscopy
non-constant force field molecular dynamics
self-assembly

Received: 27.04.2021
Revised: 07.06.2021
Accepted: 09.06.2021
Available online: 10.06.2021

1. Introduction

Oxide semiconducting glasses possess electron conductivity due to the electron transfer between ions of transition metals (V^{4+}/V^{5+}, Fe^{2+}/Fe^{3+}, Pb^{2+}/Pb^{4+}, etc.) [1–3]. Such glasses attract scientific attention because of the combination of electron conductivity and features of the vitreous state: glasses can be given any shape, and their composition can be varied in a wide range of concentrations, achieving the required properties. Glasses containing transition metal oxides can be used as electrode materials of batteries, gas sensors, for the disposal of high-level waste, etc. [4–6]. Vanadate glasses have the highest conductivity among semiconducting oxide glasses [7]; vanadate phosphate glasses are the most studied. At the same time, despite numerous works devoted to the study of vanadate-phosphate glasses in terms of their conductivity, insufficient attention has been paid to the explanation of some concentration dependence of non-electrical properties. For example, we have carried out a detailed study of the thermal and transport properties of xV_2O_5–$(1-x)P_2O_5$ (x = 35–95 mol %) glasses, and it appeared that the properties change non-linearly with vanadium content and their concentration dependences demonstrate several clearly distinguished ranges [8]. It has been suggested that the observed phenomena are connected with the structural changes of the glass network.

Vanadium glasses have a complex structure because vanadium ions can exist in four-, five- and six-coordinated states (tetrahedron, square pyramid, trigonal bipyramid, and octahedron [9]). Moreover, vanadium oxide is a transition metal which possesses at least four- and five-valent states in glasses, and ions with different valence can form the same structural groups [10]. According to [11], amorphous vanadium oxide consists of VO_4 and VO_5 structural units sharing edges and corners, while VO_4 units dominate in the molted V_2O_5 and VO_5 units are formed due to the transformation of VO_4 ones at quenching. In binary vanadium phosphate glasses, VO_4 structural units can substitute similar PO_4 units [12] forming a continuous glass network. The structure of binary V_2O_5–P_2O_5 glasses was studied in a wide composition range by NMR spectroscopy [13, 14], ESR [15], and IR spectroscopy [16]. It was established that there are two types of VO_5 units in glasses involving VO_5 units sharing oxygen with only VO_5 units and VO_5 units sharing oxygen atoms with PO_4 units [14]. The structure of glasses containing 50 mol % P_2O_5 was proven to be similar to the structure of VPO_5 crystalline compounds [17]. It was shown in [18] by studying the crystallization products of vanadium phosphate glasses that a

significant difference should be observed between the structures of glasses with compositions lying below and above 78 mol % V_2O_5. When V_2O_5 content is more than 78 mol %, the crystallization of V_2O_5 is observed; at V_2O_5 concentration below 78 mol %, the crystallization of VPO_5 solid solution is possible, which is confirmed by IR spectroscopy. According to the recent research, main vanadium structural units in binary vanadate-phosphate glasses are presented by symmetric-$V^{5+}O_4$ (s-VO_4), distorted-$V^{5+}O_4$ (d-VO_4), $V^{5+}O_6$ (VO_6), and $V^{5+}O_5$ units (VO_5) [10].

In the present work, structural models of xV_2O_5–(1-x)P_2O_5 (x = 35–95 mol %) glasses were obtained by means of self-assembly using non-constant field molecular dynamics. This method simulates the formation of glasses from a completely dissociated state by creating covalence bonds, and its applicability was demonstrated on borate-vanadate glasses [19]. The obtained models were analyzed by different structural criteria, and some quantitative factors connected with the network structure were obtained. It was shown that the bends on concentration dependences of these parameters correlate with the bends on such dependences of physicochemical properties. Similar bends were observed in the IR spectra.

2. Experimental

Glasses of the xV_2O_5–(1-x)P_2O_5 (x = 35–95 mol %) system were obtained by melt quenching by the technique described in [8]. Their amorphous nature was confirmed by X-ray diffraction using a D/Max 2200 diffractometer (Rigaku, Japan) with Cu Kα radiation (λ = 1.5418 Å) in a 2θ range of 15–55°.

To study the structural changes occurring at a change in V_2O_5/P_2O_5 ratio, infrared (IR) spectroscopy was used. The spectra were collected in the absorption mode at room temperature in a wavelength range of 400–4000 cm^{-1} using a Tensor 27 Fourier IR spectrometer (Bruker, Germany). Before measurements, glass powders were mixed with KBr in a weight ratio of 1:500, and the pellets were compacted in an evacuated mold. Then, pre-treatment (baseline subtraction) and deconvolution of the spectra into Gaussian components were performed using the Fityk software [20].

3. Simulation details

Molecular dynamics simulation was performed with CUDA version of aztotMD software [21] (the latest version and user manual are available at http://aztotmd.ru/set.php?lang=en). The computations were performed on a GeForce RTX 2080 Ti video card with a clock rate of 1650 MHz. The xV_2O_5–(100-x)P_2O_5 glass compositions with x = 35–95 mol % were studied by simulation. The starting configurations consisted of V^{5+}, P^{5+}, and O^{2-} ions, and 10% of V^{5+} ions were replaced by V^{4+} ions with the corresponding correction of the O^{2-} number. This corrective was made according to some experimental evidence. The box sizes were chosen to match the earlier obtained density data [8]. A summary of the simulated system's size is given in Table 1. The following self-assembly procedure was performed in two stages. In the first stage, V^{5+} and P^{5+} ions can form double bonds with oxygen ions O^{2-} when the distance between couples of vanadium(phosphorus) and oxygen ions is short enough. This process leads to species conversion:

$$V^{5+}/P^{5+} + O^{2-} \rightarrow V^{3+2\delta}/P^{3+2\delta} = O_d^{-2\delta} \quad (1)$$

Note that the formal oxidation degree of ions remains the same, but the partial charges are changed. $V^{3+2\delta}$ in Eq. (1) means five-valent vanadium with two electron pairs shared with the double-bonded oxygen ($O_d^{-2\delta}$). The value of δ was chosen as 0.6e, as in [22]. Hereinafter, we will omit the partial part of the charges (multiple δ) for brevity. This stage was stopped after all pentavalent cations were bonded to oxygen. In the next stage, the obtained cations as well as the remained V^{4+} cations are sequentially linked to oxygen in a similar way up to the formation of four bonds for each cation (V^{5+} and P^{5+} had one double bond and three single, V^{4+} had four singles). The oxygen ions converted sequentially into the terminal (O_t, one bond) and bridging (O_c, two bonds):

$$_dO = V^{3+}/P^{3+} + O^{2-}/O_t \rightarrow {}_dO = V^{2+}/P^{2+}–O_t/O_c, \quad (2)$$

and

$$V^{4+} + O^{2-}/O_t \rightarrow V^{3+}–O_t/O_c. \quad (3)$$

In Eq. (3), V^{3+} means $V^{3+\delta}$, not $V^{3+2\delta}$ as in Eqs. (1,2). At these stages, covalent bonds were taken in the form of harmonic potentials with the spring constant of 10-

Table 1 The simulated system sizes: nV^{5+}, nV^{4+}, nP^{5+}, and nO^{2-} are the amounts of the corresponding ions, N_{tot} is the total amount of ions, and a is the box size

x	nV^{5+}	nV^{4+}	nP^{5+}	nO^{2-}	N_{tot}	a, Å
95	854	95	50	2450	3449	36.7
90	810	90	100	2455	3455	36.8
85	764	85	150	2455	3454	36.7
80	720	80	200	2460	3460	36.6
75	674	75	250	2460	3459	36.6
70	630	70	300	2465	3465	36.5
65	584	65	350	2465	3464	36.4
60	540	60	400	2470	3470	36.4
55	494	55	450	2470	3469	36.3
50	450	50	500	2475	3475	36.2
45	404	45	550	2475	3474	36.1
40	360	40	600	2480	3480	36.0
35	314	35	650	2480	3479	36.0

30 eVÅ^{-2} and the corresponding equilibrium distance. The creation of bridging oxygen (O_c) was accompanied by adding a valent angle potential. Finally, after the self-assembly procedure, the main part of the simulation was provided during 3'000'000 steps with a timestep of 1 fs. The force field for this stage was replaced with the one from our previous work [8]. The electrostatics was calculated in a way suggested by Fennel and Gezelter [23]. In all cases, the temperature was kept around 298 K by the Nose-Hoover thermostat.

4. Results and Discussion

Fig. 1 presents the general appearance of IR spectra obtained for xV_2O_5–(1-x)P_2O_5 (x = 35–95 mol %) glasses in a wavelength range of 400–2000 cm^{-1}. It is seen that the shape of the spectra changes significantly depending on the P_2O_5/V_2O_5 ratio. The two most pronounced changes in the spectrum shape can be distinguished at x = 50 and 70 mol %. Since the last meaningful peak is observed at ~1750 cm^{-1}, the considered wavelength range was reduced to 1800 cm^{-1}. The following peaks corresponding to the vibrations of the glass network can be distinguished in the spectra: ~480, 530, 665–690, 760, 800–820, 960–980, 1040–1060, 1230, 1370, and 1750 cm^{-1}. However, these peaks are broadened, and, in most cases, they are a superposition of several peaks, as typical for amorphous materials. A slight bend is seen near ~1010 cm^{-1}, after which a sharp growth of the intensity of the spectra is observed; such behavior might be connected with the presence of bound water in samples. Therefore, the spectra were considered in two wavelengths of 400–1010 and 1010–1800 cm^{-1} to increase the deconvolution accuracy. For clarity, the peaks observed in the spectra given in Fig. 1 are listed in Table 2.

4.1. Wavelength range from 400 to 1010 cm^{-1}

As was mentioned above, several concentration ranges with the same spectrum shape exist. As V_2O_5 content grows, a redistribution of intensity is observed between the wavelength ranges of 400–650 and 850–1010 cm^{-1}.

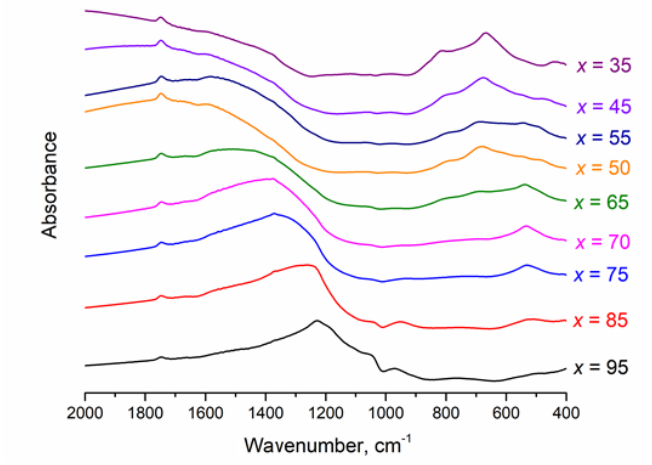

Fig. 1 IR spectra of xV_2O_5–(100-x)P_2O_5 glasses

Table 2 Peaks observed in IR spectra (see Fig. 1)

Wavenumber, cm^{-1}	Vibration type	Reference
475–490	δ O–P–O	[24, 25]
530	δ O=P–O	[25, 26]
665–690	ν_s O–P–O	[26]
760	ν_s V–O–P; ν_s P–O–P	[25]
800–820	ν_s P–O–P	[26]
960–980	V–O	[25]
1040–1060	V=O	[27, 28]
1230	ν_s P=O (Q^2)	[24, 25]
1370	ν_{as} P=O (Q^2)	[26]

For the middle of the spectra (650–850 cm^{-1}), no strong correlation between the glass composition and peak intensity is observed; however, its shape depends on the glass composition: when V_2O_5 concentration is reduced from 95 mol %, the peak becomes smoother, and it almost disappears at V_2O_5 content of 70 mol %.

The examples of deconvolution of the spectra in this area are given in Fig. 2. According to the literature data, bending vibrations of V–O–V bonds are observed in the wavelength range of 400–650 cm^{-1}, as well as various vibrations of phosphate glass network, for example, vibrations of O–P–O and O=P–O bonds [29–31]. Considering that the intensity of this peak increases as P_2O_5 content grows, the main contribution might be assigned to the vibrations of PO_2^- structural units [24, 31].

In the wavelength range of 650–850 cm^{-1}, a gradual degeneration of the most intense peak is observed, and it shifts towards lower wavelengths (from 757 to 742 cm^{-1} for V_2O_5 content of 95 and 75 mol %, respectively). The following vibrations can be excited in this spectrum area: stretching vibrations of P–O–P [24, 31] and V–O–P [32] bonds and the vibrations of the vanadium-oxygen network such as asymmetric stretching vibrations of VO_2 groups in VO_4 tetrahedra [30, 33]. Since the vibrations of phosphate and vanadate networks in this area are overlapped, it is complicated to unambiguously relate the peaks obtained by spectra deconvolution. It might be assumed that the main contribution to the intensity of the peak at ~750 cm^{-1} is made by the vibrations of the vanadium-oxygen network, as well as V–O–P vibrations, in the V_2O_5 concentration range from 85 to 95 mol %. As P_2O_5 content increases, this peak shifts towards the low-frequency area, which is followed by its vanishing; that may be connected with both a low intensity of vanadium-oxygen network vibration and restructuring of the glass network (transition from predominantly vanadate to mixed phosphate-vanadate glass network).

Within the wavelength range of 850–1010 cm^{-1}, the most noticeable changes occur at V_2O_5 content of 80 mol %. In the 85 ≤ x ≤ 95 (mol %) composition range, three peaks are observed in the spectra deconvolution: ~985, 965, and 933 cm^{-1}. The intensity of the peak at 985 cm^{-1} remains the same within this V_2O_5 range, while the intensity is redistributed between the peaks at 933 and 965 cm^{-1}. The peak at 965 cm^{-1} can be attributed to the stretching vibrations of V–O bonds in VO_4 structural units [29].

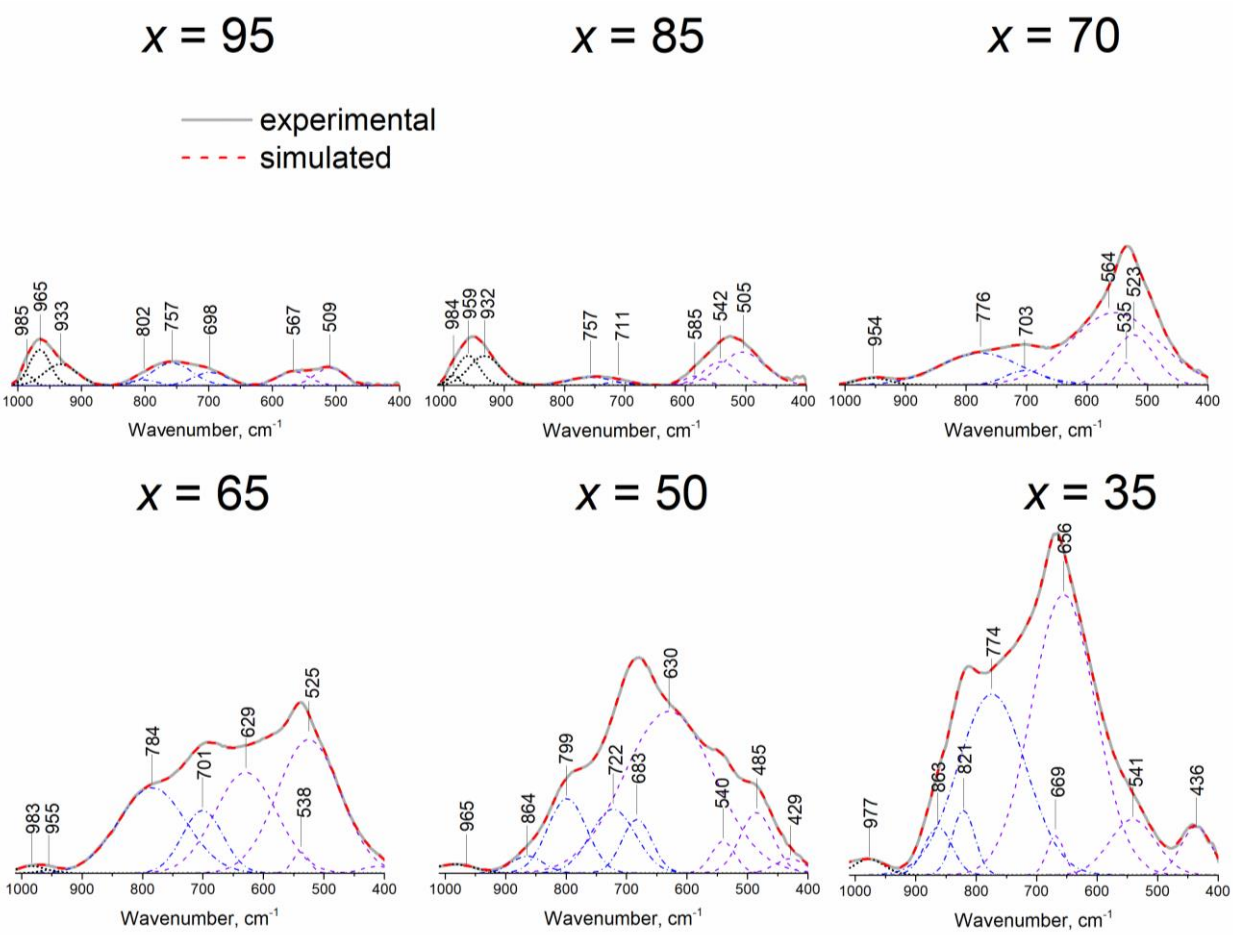

Fig. 2 Deconvolution of IR spectra of $x V_2O_5$–(100-x)P_2O_5 glasses in the wavelength range of 400–1010 cm^{-1}. The spectra are plotted in the same ranges on the y-axis to demonstrate the intensity change.

Hence, decreasing its intensity is connected with the reduction of vanadium oxide concentration and, consequently, the number of bonds formed with vanadium ions. The peak at ~935 cm^{-1} is connected with the stretching vibrations of P–O–P bonds in Q^0 structural units [29, 34–36]; therefore, the growth of its intensity is also natural.

It is interesting to mention the peak at 985 $cm^{-1,}$ which vanishes with decreasing the V_2O_5 content from 95 to 80 mol %. According to the literature data, it can be caused by the vibrations of vanadium-oxygen tetrahedra VO_4 [37], constituting the glass network at high vanadium oxide content [38], or vanadium clusters [37]. Probably, the glass network changes drastically with the growth of P_2O_5 content, which results in the decay of vanadium clusters.

As was mentioned above, a change in the shape of the spectra begins at V_2O_5 content of 70 mol %, which is accompanied by the disappearance of a number of peaks and redistribution of vibration intensities; this change finishes at x = 65 mol % (Fig. 2). Apparently, the transition from predominantly vanadate to mixed phosphate-vanadate glass network occurs. Beginning from x = 85 mol %, there is a peak at ~530–540 cm^{-1}, whose intensity and position are kept with a further increase in P_2O_5 concentration. This indicates that this peak is attributed to the vibrations of the phosphate structural units.

More noticeable changes in the shape of the spectra occur in the wavelength range of 650–900 cm^{-1}. The intensity of peaks in the area of 650–850 cm^{-1} increases sharply; the position of the peak at ~700 cm^{-1} observed for the glass with x = 70 mol % is almost unchanged, while the peak with the maximum at ~780 cm^{-1} shifts towards larger wavenumbers. The vibrations in this spectrum area are attributed to the symmetric stretching vibrations of P–O–P bonds in Q^2 structural groups [39–42]. The growth of the intensity of these peaks clearly indicates increasing the connectivity of the phosphate network with an increase in P_2O_5 content.

The peak at ~700 cm^{-1} appears in the spectra of glass with x = 70 mol % and maintains with the P_2O_5 content growth up to x = 55 mol %; in the spectrum of x = 50 mol % composition, this peak completely disappears. According to the literature data [26], this peak is typical for P–O–P vibrations and symmetric stretching vibrations of phosphate rings [25]. The peak near ~780 cm^{-1} arises for the composition with x = 70 mol % and persists up to the maximum P_2O_5 concentration shifting towards large wavenumbers (821 cm^{-1}). This peak could be caused by symmetric stretching vibrations of P–O–P bonds in Q^2 groups [39–42].

Further distortion of the spectrum shape begins at V_2O_5 content of 55 mol % and ends at x = 50 mol %. A slight narrowing of the top of the spectra accompanied by a redistribution of intensity of vibrations in all studied wavelength range is observed.

The appearance of the peak at 488 cm^{-1} can be mentioned in the spectra of glasses with x = 55 mol %; this peak shifts to the low-frequency area as P_2O_5 content grows. This peak may be attributed to the bending vibrations of PO_4 tetrahedra [43]. Its appearance indicates the formation of the metaphosphate chain with decreasing V_2O_5 content, which indirectly indicates the modifying role of V_2O_5 in this concentration range.

The peak near 620–640 cm^{-1} becomes more pronounced, and it shifts towards the high-frequency area with the growth of P_2O_5 concentration (660–690 cm^{-1}). In this area, bending vibrations of O–P–O bonds [43] and stretching vibrations of P–O–P bonds [44] are observed. Increasing the intensity of this peak indicates the growth of connectivity of the phosphate network and the possible formation of this network with inclusions of vanadium-oxygen clusters. This suggestion is indirectly confirmed by the constancy of the peak near 980–990 cm^{-1}, whose appearance points up the existence of vanadium-oxygen clusters in the glass network [31].

4.2. Wavelength range from 1010 to 1800 cm^{-1}

In the wavelength range of 1010–1800 cm^{-1}, changes in the shape and intensity of the spectra are similar to those observed in the 400–1010 cm^{-1} range. The broadening of the spectra is observed in this frequency range as the P_2O_5 content increases (Fig. 1). This might be connected with the growth of hygroscopicity of glasses with an increase in P_2O_5 and, consequently, a large amount of bound water in the glass structure. It can cause a broadening of the spectrum associated with the absorption of water molecules and the appearance of P–OH bonds. For these reasons, unambiguous interpretation of the results of spectrum deconvolution is difficult; therefore, only a brief discussion of the peaks which can be interpreted based on the literature data is given below.

The peaks at ~1230–1270 and 1350–1370 cm^{-1} are present in the spectra of all studied compositions (Fig. 3), and they can be attributed to the vibrations of P=O bonds [45]. In addition, there is a peak at ~1040–1060 cm^{-1}, which indicates the vibrations of V=O bonds [46] or asymmetric stretching vibrations of pyrophosphate groups [47]; its intensity decreases with the growth of P_2O_5 content. A small peak at ~1745 cm^{-1} is likely connected with the vibrations of the OH groups [48]. The rest of the peaks in the range of 1400–1800 cm^{-1} are assigned to the vibrations of P–OH bonds and adsorbed water molecules [48].

4.3. Simulation results

Examples of snapshots of the simulated systems are given in Fig. 4; for clarity, we presented only thin slices of the systems cut from the middle of the box. One can see phosphate-vanadate chains and valent angles R-O-R. The interatomic distances correspond to experimental data on single and double bond lengths, as was shown in detail in our

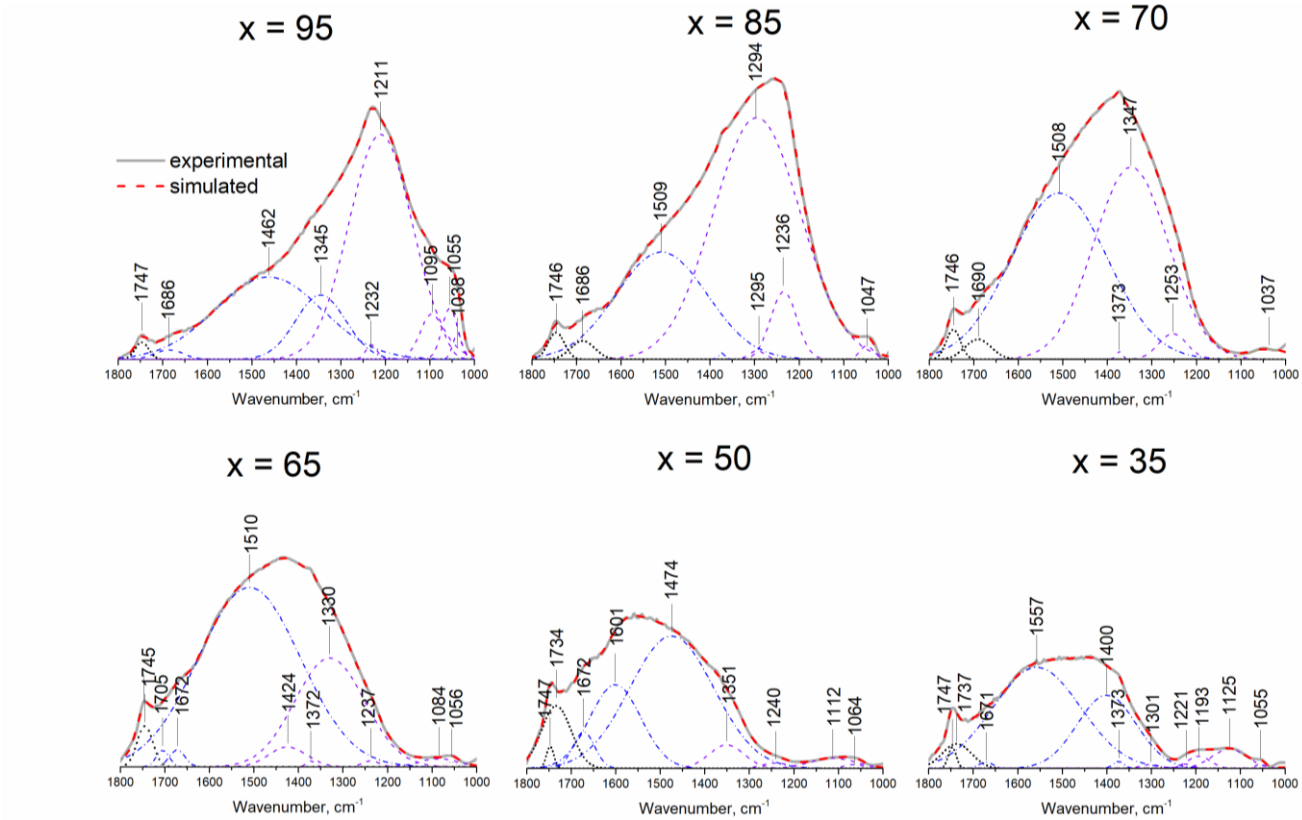

Fig. 3 Deconvolution of IR spectra of $x$$V_2O_5$–(100-$x$)$P_2O_5$ glasses in the wavelength range of 1000–1800 cm^{-1}. The spectra are plotted in the same range on the y-axis to demonstrate the intensity change.

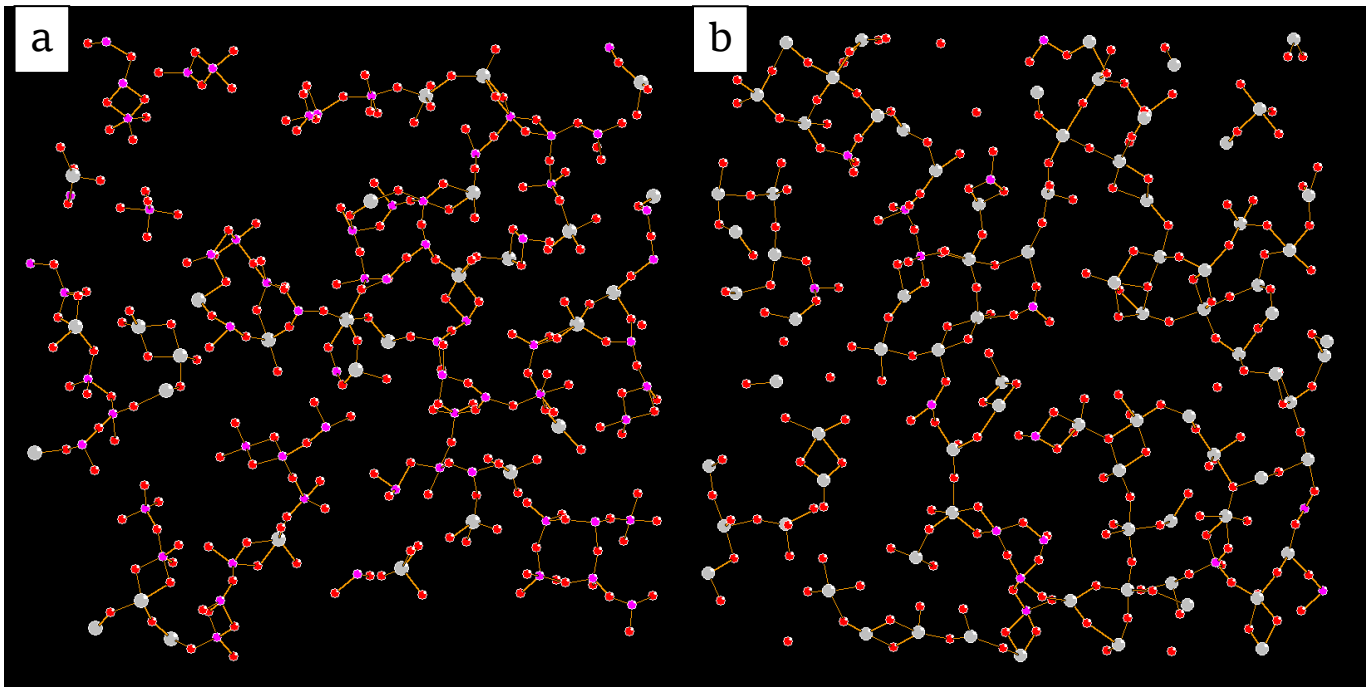

Fig. 4 Snapshots of the simulated xV$_2$O$_5$–(100-x)P$_2$O$_5$ glasses (thin slices) for (a) x = 35 and (b) x = 80 mol %. Colors: magenta – P, gray – V, red – O.

previous work [8]. Fig. 5 shows distributions of vanadium ions by coordination number (at a cutoff of 2.21 Å) and mean coordination number as a function of vanadium content. The dominated coordination is five (about 60%), and, in general, the proportion of four-coordinated vanadium decreases, and that of six-coordinated increases with an increase in vanadium content.

To estimate the structure of the glass network, we analyzed the number of atoms with different quantities of triatomic bond sequences; for this purpose, we introduced R^n_{OR} notation, where n is the number of R–O–R bonds starting from a given atom R, see Fig. 6 for the explanation. Fig. 7 shows the dependences of P^n_{OP} as a percentage of the total number of P atoms; for example, P^2_{OP} = 30% means that 30% of phosphorous atoms have exactly two bonds P–O–P starting from them. All R^n_{OR} values are averaged over five final configurations. Fraction of P^4_{OP} (all surroundings are phosphate) is about 5% even at the highest P_2O_5 content and almost disappears at x = 70 mol %. P^0_{OP} (all atoms in the second coordination sphere are vanadium) grows from 12 to 85 %, and this concentration dependence can be divided into three regions (x = 35–50, 55–70, and 75–95 mol %) with the increasing slope. Starting from x = 75 mol %, more than half of the phosphorous atoms are surrounded by vanadium. The dependence of P^1_{OP} (single P–O–P clusters inside of the vanadate matrix) passes through the maximum. Fraction of these units grows up to the point x = 50 mol % and then, after x = 65 mol % falls, i.e., initially dilution of the system by vanadium leads to breaking of the phosphate network with the creation of single clusters, and then they also disappear.

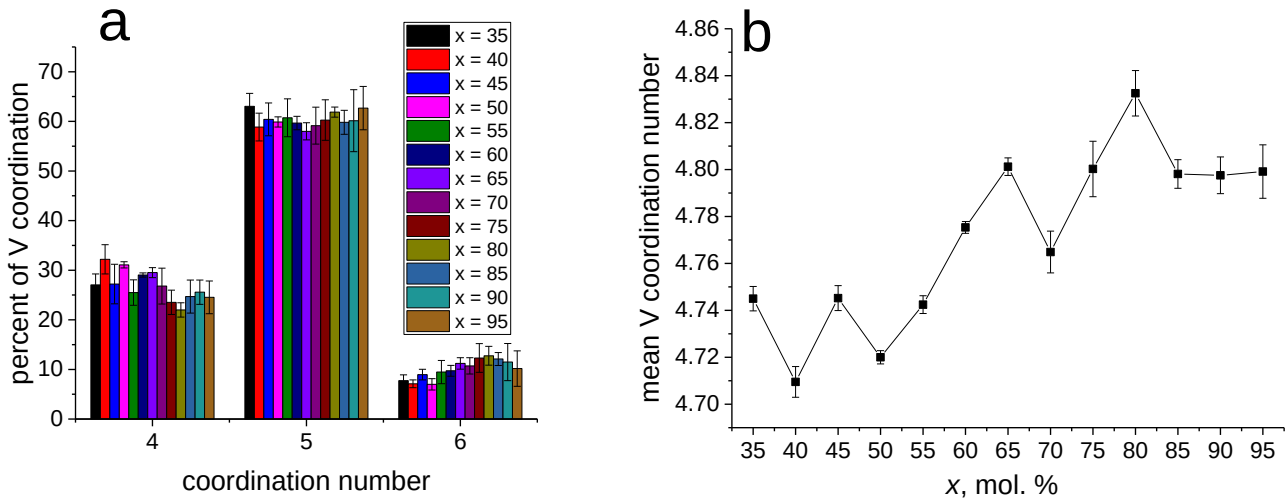

Fig. 5 (a) Distributions of vanadium ions by coordination number (at cutoff of 2.21 Å) for different compositions and (b) mean coordination number as a function of vanadium content

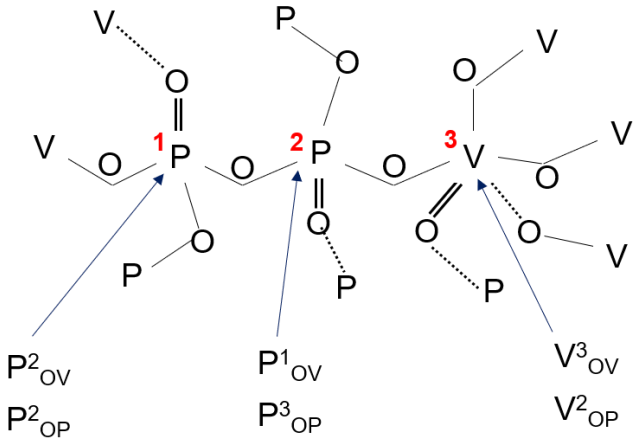

Fig. 6 Explanation of R^n_{OR} notation: P atom labeled "1" has two bonds with vanadium (via oxygen) and two bonds with phosphorous (via oxygen), so it can be indicated P^2_{OV} as well as P^2_{OP}. Similarly, the 2nd atom is P^1_{OV}/P^3_{OP}, and 3rd is V^3_{OV}/V^2_{OP}

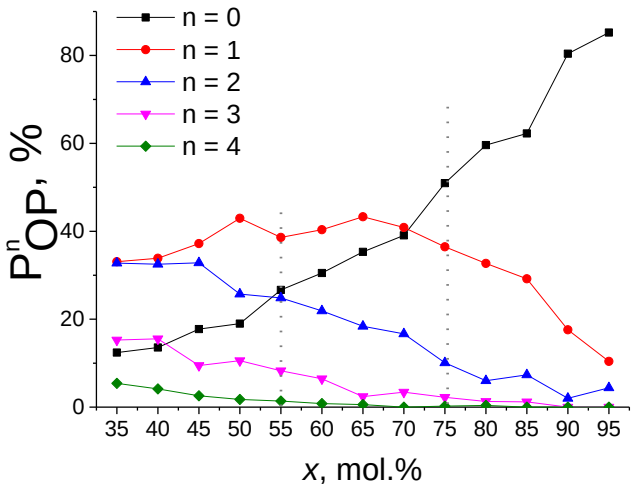

Fig. 7 Fraction of P^n_{OP} as a function of vanadium oxide content for simulated xV_2O_5–(100-x)P_2O_5 glasses

The fraction of vanadium fully surrounded by phosphorous (V^0_{OV}) falls with increasing of V_2O_5 content and disappears starting from x = 80 mol %, Fig. 8. The numbers of isolated (V^1_{OV}) and "chained" (V^2_{OV}) vanadate fragments also fall. The fraction of V^3_{OV} passes through the maximum at x = 60 mol %, V^4_{OV} grows sigmoidal and reaches a plateau value of ~1/3 at x = 75 mol %. This coordination dominates up to x = 90 mol %, and then V^5_{OV} dominates. V^6_{OV} increases weakly and reaches values about 7% at x = 95 mol %. This fact is related to the vanadium coordination number. Unlike phosphorous, vanadium coordination numbers can vary from 4 to 6, and V^4_{OV} may mean that vanadium has only four V–O–V bonds as well as more than four bonds, and only four of them are V–O–V.

It is interesting that P^2_{OV} fluctuates around 30% for all studied compositions but two last, i.e., every third P atom has two P–O–V bonds, Fig. 9. The fraction of P atoms without P–O–V bonds (P^0_{OV}) drops dramatically down to the value of 2.4% at x = 65 mol %, then decreases smoothly and disappears around x = 85 mol %.

According to Fig. 10, the number of vanadium atoms without connection with phosphorous (V^0_{OP}) grows from ~5 to 85%. V^6_{OP} is about zero for all compositions (is not shown in figures). Comparison with Fig. 8, which shows that isolated vanadate units still exist, one can conclude that V atoms, which are linked only to P atoms, have coordination less than 6. V^5_{OP} almost disappears from x = 60 mol %, V^4_{OP} – from x = 80 mol %. V^1_{OP} passes through the maximum at x = 75 mol %.

In addition, we analyzed the obtained configurations for 4-, 6- and 8-membered cycles using the written script. The preliminary results, averaged over five configurations, are summarized in Table 3. As one can see from the table, the total number of cycles, as well as the number of participated in cycles atoms, grows with increasing of V_2O_5 content. It is interesting that 4-membered cycles were detected. In terms of coordination polyhedra, such cycles mean that two coordination polyhedra have a shared edge, not a corner which is against Zachariasen's rule [49].

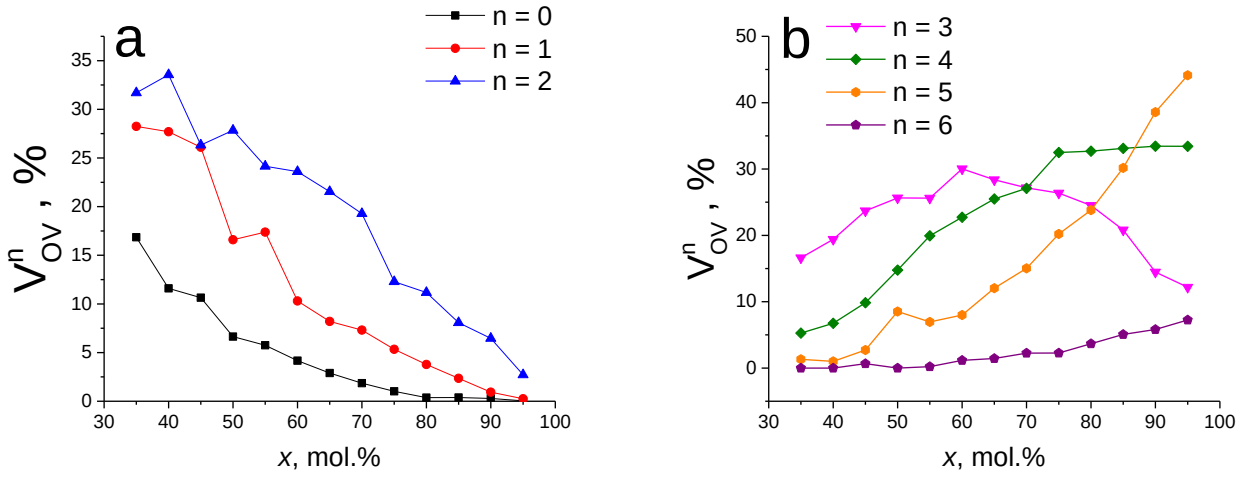

Fig. 8 Fraction of V^n_{OV} as a function of vanadium oxide content for simulated xV_2O_5–(100-x)P_2O_5 glasses: (a) n = 0–2 and (b) n = 3–6

Fig. 11(a) demonstrates the number of R–O–R–O cycles related to the number of corresponding atoms; these fractions directly correlate with the amount of phosphorous/vanadium in the system. However, the formation of 4-membered cycles is less typical for phosphorous than for vanadium. Even at high P_2O_5 content, less than 5% of phosphorous participates in such cycles. One can conclude that phosphorous oxide obeys Zachariasen's rule strictly than vanadium oxide. This leads to the fact that P_2O_5 is the main glass former and V_2O_5 is an intermediate. In general, vanadium is more prone to form cycles due to higher coordination numbers and longer V–O bonds.

Fig. 11(b) shows the dependences of the number of 6-membered cycles normalized to the total number of P and V atoms. Here is also evident that vanadium tends to form cycles better than phosphorous. Even at the equimolar ratio of the oxides in the glass (x = 50 mol %), the dominated cycle's species is VVP. Starting from x = 55 mol %, the numbers of the VVV and VVP cycles are comparable, and from x = 70 mol %, the VVV cycles become dominated among 6-membered cycles. Examples of the found cycles are given in Fig. 12.

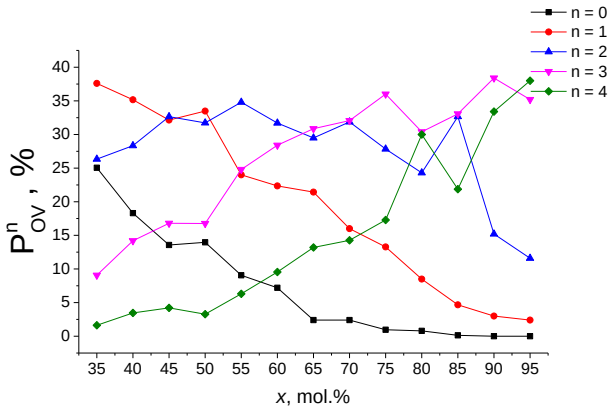

Fig. 9 Fraction of P^n_{OV} as a function of vanadium oxide content for simulated xV_2O_5–(100-x)P_2O_5 glasses

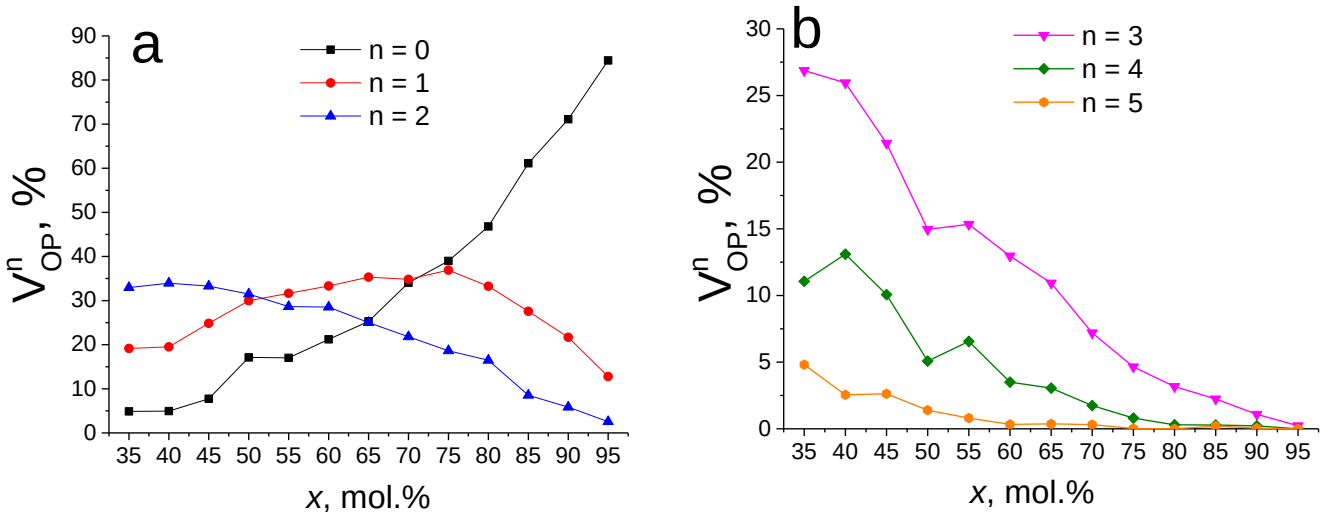

Fig. 10 Fraction of V^n_{OP} as a function of vanadium oxide content for simulated xV_2O_5–(100-x)P_2O_5 glasses

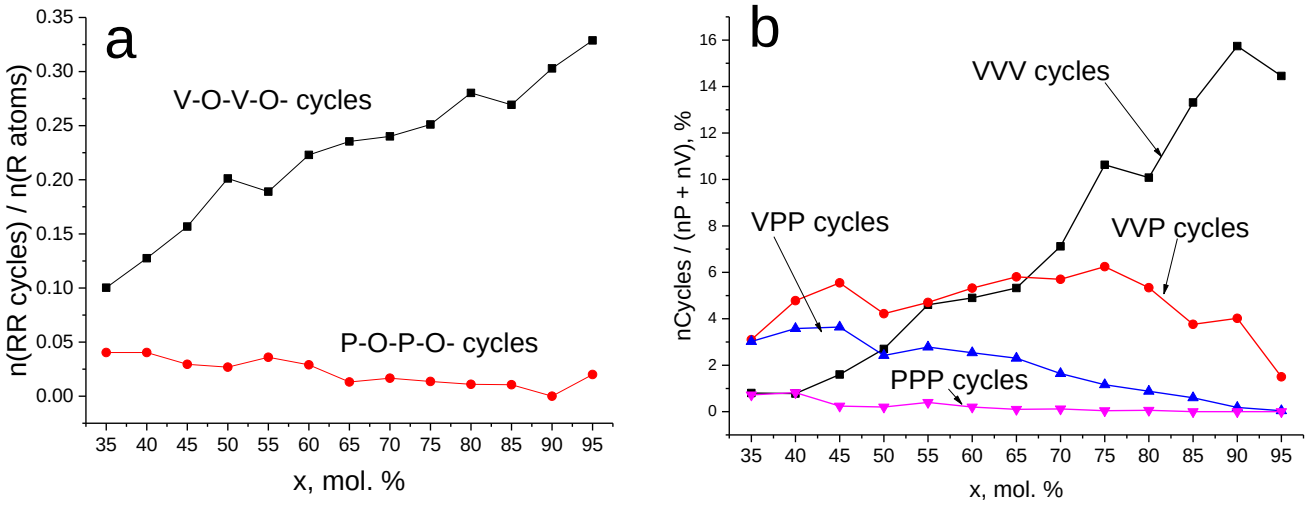

Fig. 11 (a) Number of R–O–R–O cycles normalized per number of corresponding elements as a function of vanadium content and (b) the number of 6-membered cycles of each type normalized per sum of vanadium and phosphorous atoms

Table 3 Statistics by cycles: number of cycles (*nC*), number of atoms participated in cycles (*nAt*) and number of each cycle (as a percentage of the total cycle number). The record VV means V–O–V–O– cycle, VP means V–O–P–O– cycle, etc.

x	*nC*	*nAt*	VV	VP	PP	VVV	VVP	VPP	PPP	VVVV	VVVP	VPVP	VVPP	VPPP	PPPP
35	317.8	1258.2	11.0	21.9	8.2	2.5	9.7	9.5	2.3	2.4	6.5	4.2	7.7	10.8	3.2
40	394.0	1485.4	12.9	21.4	6.1	2.0	12.1	9.1	2.1	0.8	8.7	5.0	8.9	8.4	2.4
45	406.4	1446.4	17.3	18.1	4.0	3.9	13.6	9.0	0.6	2.9	12.5	2.8	9.2	5.5	0.5
50	368.0	1344.6	27.3	14.9	3.6	7.3	11.5	6.6	0.5	4.6	9.5	3.3	6.4	4.1	0.3
55	445.2	1559.6	23.3	15.8	3.6	10.3	10.6	6.2	0.9	7.0	12.1	2.3	4.6	3.0	0.2
60	506.6	1700.8	26.4	13.3	2.3	9.7	10.5	5.0	0.4	6.4	15.4	2.8	6.4	1.2	0.2
65	556.4	1803.0	27.5	15.4	0.8	9.6	10.4	4.1	0.2	11.3	11.7	1.0	6.6	1.4	0.0
70	557.4	1901.6	30.1	10.6	0.9	12.8	10.2	2.9	0.2	10.2	13.4	3.0	4.2	1.3	0.1
75	650.6	2026.8	28.9	8.3	0.5	16.3	9.6	1.8	0.1	14.9	15.1	1.5	2.4	0.5	0.1
80	697.2	2087.4	32.2	8.2	0.3	14.4	7.6	1.3	0.1	19.8	13.9	0.0	2.1	0.0	0.0
85	690.8	2109.0	33.1	4.5	0.2	19.2	5.4	0.9	0.0	24.6	9.4	1.0	1.6	0.1	0.0
90	775.8	2293.8	35.1	4.4	0.0	20.3	5.2	0.2	0.0	26.3	7.8	0.5	0.2	0.0	0.0
95	772.4	2302.6	40.4	1.6	0.1	18.7	1.9	0.1	0.0	32.4	4.4	0.0	0.4	0.0	0.0

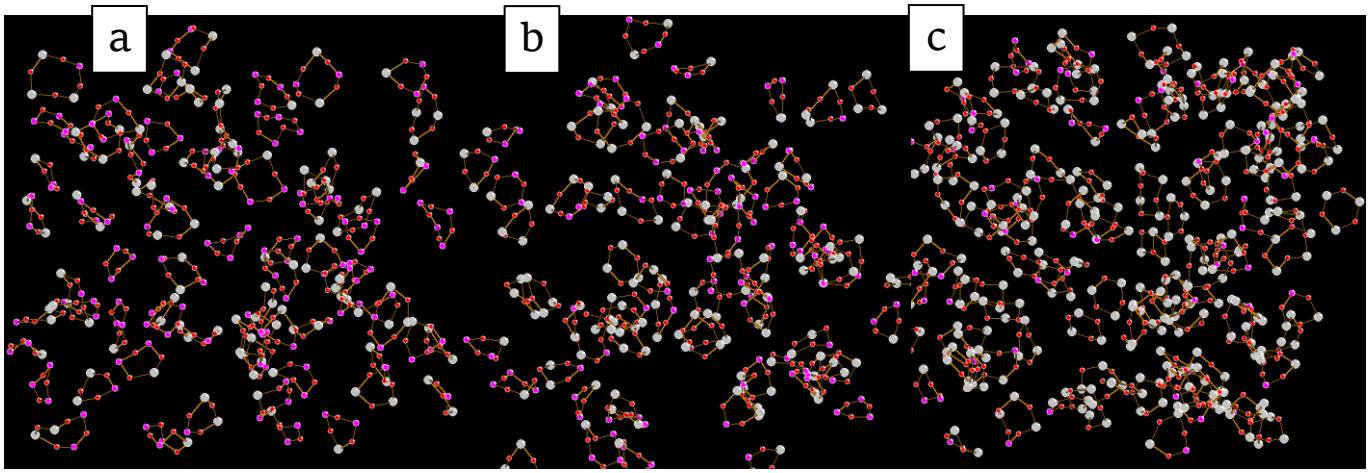

Fig. 12 Examples of found 6- and 8-membered cycles in the simulated $x V_2O_5$-(100-x)P_2O_5 glasses for (a) x = 35, (b) x = 50 and (c) x = 80 mol %. Only atoms participating in the cycles are shown. Colors: magenta – P, gray – V, red – O.

4.4. Connectivity of structure and properties

It was mentioned above that some intervals of V_2O_5 content can be distinguished by the spectrum shape, namely, 95–70, 65–55, and 50–35 mol % V_2O_5. Observed structural changes agree well with the concentration dependences of other physicochemical properties of the xV_2O_5–(100-x)P_2O_5 glasses found earlier [8]. A bend was observed in the concentration dependence of glass transition temperature in the area of x = 65–70 mol % (Fig. 13a). It was suggested that this effect could be explained by changing the glass structure, for example, by the transition from predominant vanadium-oxygen units to a mixed vanadium-phosphate network with a predominance of phosphate structural units. According to the IR spectroscopy results, a noticeable restructuring is observed in this range of V_2O_5 concentration which agrees with our hypothesis. It was confirmed by the simulation results (Fig. 13a): above x = 65 mol %, phosphorous atoms without vanadium ones in the second coordination sphere are almost absent. When x < 65 mol %, the number of such phosphorous atoms sharply increases, i.e., isolated phosphorous clusters are formed (Fig. 9).

Moreover, a change in conductivity behavior was observed in the same range of V_2O_5 concentrations which was expressed as a change in the impedance spectra shape and a sudden decrease in conductivity (Fig. 13b). It was assumed that such behavior is connected with a change in the charge transfer mechanism in the studied glasses. Based on the data on the structure of phosphate-vanadate glasses, one can assume that structural changes strongly affected the conductivity. Similar changes were observed at x = 45–50 mol % that can also be explained by the change of the glass network from mixed to predominantly phosphate with vanadium-oxygen clusters. When x < 50 mol %, the number of phosphorous atoms with two bonds P–O–P (which could be considered as phosphate chains with vanadate branches) is about a third of all phosphorus atoms, and it decreases with the x growth (Fig. 7). Moreover, it is seen that at x = 50 mol %, a sharp increase in the fraction of phosphorus atoms isolated by the vanadate matrix begins. Thus, it can be concluded that the observed deviations in the concentration dependences of some physicochemical properties of xV_2O_5–(100-x)P_2O_5 glasses can be explained by the detailed investigation of their structure by IR spectroscopy combined with the analysis of atomic configurations obtained by molecular simulation.

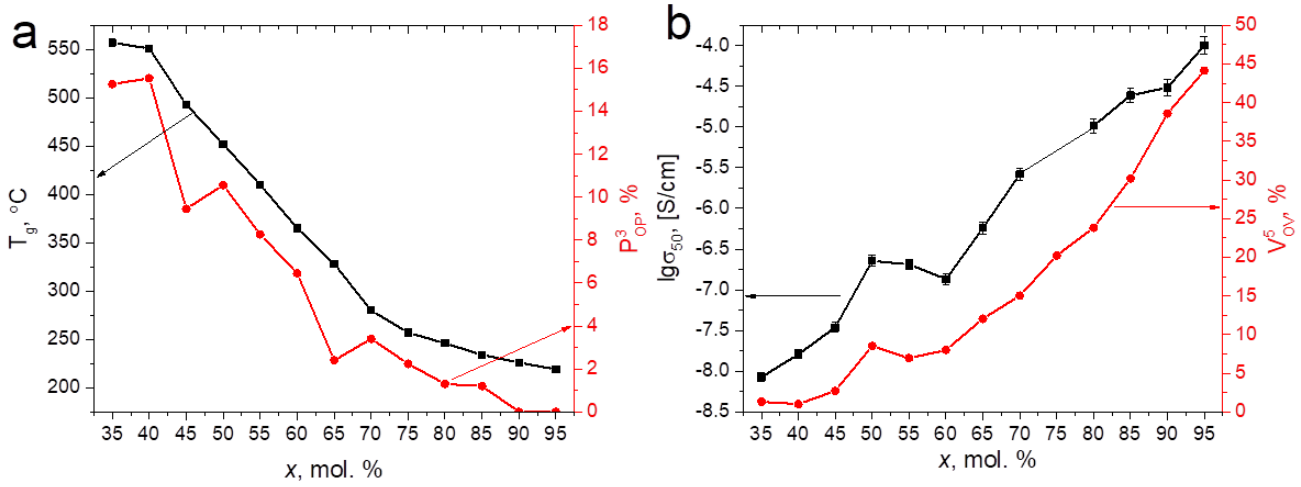

Fig. 13 (a) concentration dependences of glass transition temperature (T_g) and P^3_{OP} cycles and (b) concentration dependences of $lg\sigma_{50}$ and V^5_{OV} cycles. Data on glass transition temperature and electrical conductivity are taken from [8]

5. Conclusions

xV_2O_5–(100-x)P_2O_5 (x = 35–95 mol %) glasses were studied by IR spectroscopy. By means of deconvolution of the IR spectra, the data were obtained on changes in the glass structure, and the correlation of these changes with a number of physicochemical properties was shown. To obtain the structural models of the glasses, self-assembly was performed using non-constant field molecular dynamics. The models were analyzed to find the atom distribution by the number of defined triatomic sequences. Bends and kinks are observed in their concentration dependences, which indicate the transitions between the main glass-forming elements. These points coincide with the changes observed in the IR spectra.

It was established from the analysis of obtained molecular configurations of glasses in the presence of cycles that the vanadate fragments are much more prone to the ring formation, including 4-membered cycles. According to Zachariasen's rule, systems with 4-membered cycles (edge connected coordination polyhedra) cannot have a strong tendency to vitrification. So, our results can explain why V_2O_5 has much lower glass-forming ability than P_2O_5 (melts enriched with vanadium require higher cooling rate to vitrify).

Acknowledgements

The research was supported by the Russian Science Foundation (project no. 18-73-10205).

References

1. El-Damrawi G, Abdelghany AM, Hassan AK, Faroun B. Conductivity and morphological studies on iron borosilicate glasses. J Non Cryst Solids. 2020;545:120233. doi:10.1016/j.jnoncrysol.2020.120233
2. Kaur N, Khanna A, Fábián M, Dutt S. Structural and electrical characterization of semiconducting xCuO-(100-x)TeO2 glasses. J Non Cryst Solids. 2020;534:119884. doi:10.1016/j.jnoncrysol.2020.119884
3. Ningthemcha RKN, Biswas D, Singh YB, Sarkar D, Mondal R, Mandal D, et al. Temperature and frequency dependent electrical conductivity and dielectric relaxation of mixed transition metal doped bismuth-phosphate semiconducting glassy systems. Mater Chem Phys. 2020;249:123207. doi:10.1016/j.matchemphys.2020.123207
4. Afyon S, Krumeich F, Mensing C, Borgschulte A, Nesper R. New high capacity cathode materials for rechargeable Li-ion batteries: Vanadate-borate glasses. Sci Rep [Internet]. 2014;4:7113. doi:10.1038/srep07113
5. Kaur N, Khanna A, Kaur R, Ruchika, Salhotra D. Synthesis and characterization of vanadium and iron tellurite glasses for applications as thermal sensors. Solid State Sci. 2021;114:106564. doi:10.1016/j.solidstatesciences.2021.106564
6. Li X, Xiao Z, Luo M, Dong X, Du T, Wang Y. Low melting glasses in ZnO-Fe_2O_3-P_2O_5 system with high chemical durability and thermal stability for sealing or waste immobilization. J Non Cryst Solids. 2017;469:62–9. doi:10.1016/j.jnoncrysol.2017.04.023
7. Raskovalov AA, Saetova NS. All-solid-state batteries based on glass-ceramic lithium vanadate. Solid Electrolytes Adv Appl. Springer; 2019. p. 297–334.
8. Saiko IA, Saetova NS, Raskovalov AA, Il'ina EA, Molchanova NG, Kadyrova NI. Hopping conductivity in V_2O_5-P_2O_5 glasses: Experiment and non-constant force field molecular dynamics. Solid State Ionics. 2020;345:115180. doi:10.1016/j.ssi.2019.115180
9. Hoppe U, Wyckoff NP, Schmitt ML, Brow RK, Schöps A, Hannon AC. Structure of V_2O_5-P_2O_5 glasses by X-ray and neutron diffraction. J Non Cryst Solids. 2012;358:328–36. doi:10.1016/j.jnoncrysol.2011.09.038
10. Aoyagi T, Kohara S, Naito T, Onodera Y, Kodama M, Onodera T, et al. Controlling oxygen coordination and valence of network forming cations. Sci Rep. 2020;10:7178. doi:10.1038/s41598-020-63786-y
11. Nabavi M, Sanchez C, Livage J. Structure and properties of amorphous V_2O_5. Philos Mag B Phys Condens Matter; Stat Mech Electron Opt Magn Prop. 1991;63:941–53. doi:10.1080/13642819108205549
12. Feltz A, Unger B. Redox reactions in condensed oxide systems II. Variation of the structure of vanadium phosphate glasses in dependence on the oxidation state of vanadium. J Non Cryst Solids. 1985;72:335–43. doi:10.1016/0022-3093(85)90188-7
13. Wadsworth M, France PW. Nmr quadrupole interactions in vanadium phosphate glass. J Phys C Solid State Phys. 1986;19:7129–43. doi:10.1088/0022-3719/19/36/005
14. Landsberger FR, Bray PJ. Magnetic resonance study of the V_2O_5-P_2O_5 semiconducting glass system. J Chem Phys. 1970;53:2757–68. doi:10.1063/1.1674400

15. Livage J, Pineau P, Leroy MC, Michaud M. Semiconducting vanadium phosphate glasses. Phys status solidi. 1977;39:73–8. doi:10.1002/pssa.2210390107
16. Bhargava RN, Condrate RA. Vibrational spectra of VPO_5 crystal phases and related glasses. Appl Spectrosc. 1977;31:230–60. doi:10.1366/000370277774463742
17. Gopal R, Calvo C. Crystal structure of βVPO_5. J Solid State Chem. 1972;5:432–5. doi:10.1016/0022-4596(72)90089-8
18. Sakurai Y, Yamaki J. Correlation between microstructure and electrochemical behavior of amorphous V_2O_5-P_2O_5 in lithium cells. ChemInform. 1988;19:791–6. doi:10.1002/chin.198831013
19. Saetova NS, Raskovalov AA, Il'ina EA, Antonov BD, Grzhegorzhevskii KV. Structure and electrical conductivity of glasses $30Na_2O–xV_2O_5–(70–x)B_2O_3$: Experiment and molecular dynamics with self-assembly elements. Russ J Inorg Chem. 2021;66:313–23. doi:10.1134/S003602362103013X
20. Wojdyr M. Fityk: A general-purpose peak fitting program. J Appl Crystallogr. 2010;43:1126–8. doi:10.1107/S0021889810030499
21. Raskovalov AA. azTotMD: Software for non-constant force field molecular dynamics. SoftwareX. 2019;10:100233. doi:10.1016/j.softx.2019.04.005
22. Pedone A, Malavasi G, Menziani MC, Cormack AN, Segre U. A new self-consistent empirical interatomic potential model for oxides, silicates, and silicas-based glasses. J Phys Chem B. 2006;110:11780–95. doi:10.1021/jp0611018
23. Fennell CJ, Gezelter JD. Is the Ewald summation still necessary? Pairwise alternatives to the accepted standard for long-range electrostatics. J Chem Phys. 2006;124:234104. doi:10.1063/1.2206581
24. Stefan R, Simedru D, Popa A, Ardelean I. Structural investigations of V_2O_5-P_2O_5-CaO glass system by FT-IR and EPR spectroscopies. J Mater Sci. 2012;47:3746–51. doi:10.1007/s10853-011-6225-x
25. Vedeanu N, Stanescu R, Filip S, Ardelean I, Cozar O. IR and ESR investigations on V_2O_5-P_2O_5-BaO glass system with optoelectronic potential. J Non Cryst Solids. 2012;358:1881–5. doi:10.1016/j.jnoncrysol.2012.05.010
26. Ahsan MR, Uddin MA, Mortuza MG. Infrared study of the effect of P_2O_5 in the structure of lead silicate glasses. Indian J Pure Appl Phys. CSIR; 2005;43:89–99.
27. Sindhu S, Sanghi S, Agarwal A, Seth VP, Kishore N. Structural, optical, physical and electrical properties of V_2O_5·SrO·B_2O_3 glasses. Spectrochim Acta - Part A Mol Biomol Spectrosc. 2006;64:196–204. doi:10.1016/j.saa.2005.06.039
28. Sindhu S, Sanghi S, Agarwal A, Sonam, Seth VP, Kishore N. The role of V_2O_5 in the modification of structural, optical and electrical properties of vanadium barium borate glasses. Phys B Condens Matter. 2005;365:65–75. doi:10.1016/j.physb.2005.04.037
29. Yadav AK, Singh P. A review of the structures of oxide glasses by Raman spectroscopy. RSC Adv. 2015;5:67583–609. doi:10.1039/c5ra13043c
30. Lewandowska R, Krasowski K, Bacewicz R, Garbarczyk JE. Studies of silver-vanadate superionic glasses using Raman spectroscopy. Solid State Ionics. 1999;119:229–34. doi:10.1016/S0167-2738(98)00508-6
31. Vedeanu NS, Cozar IB, Stanescu R, Stefan R, Vodnar D, Cozar O. Structural investigation of V_2O_5-P_2O_5-K_2O glass system with antibacterial potential. Bull Mater Sci. 2016;39:697–702. doi:10.1007/s12034-016-1214-y
32. Garbarczyk JE, MacHowski P, Wasiucionek M, Tykarski L, Bacewicz R, Aleksiejuk A. Studies of silver-vanadate-phosphate glasses by Raman, EPR and impedance spectroscopy methods. Solid State Ionics. 2000;136–137:1077–83. doi:10.1016/S0167-2738(00)00504-X
33. Khattak GD, Mekki A, Siddiqui MN. Compositional dependence of DC electrical conductivity of SrO-vanadate glasses. Solid State Ionics. 2012;211:5–11. doi:10.1016/j.ssi.2012.01.012
34. Toloman D, Biris AR, Maniu D, Bratu I, Giurgiu LM, Biris AS, et al. Phosphate glassy network depolymerization induced by CaO doping. Part Sci Technol. 2010;28:226–35. doi:10.1080/02726351.2010.481581
35. Galliano PG, López JMP, Varetti EL, Sobrados I, Sanz J. Analysis by nuclear magnetic resonance and raman spectroscopies of the structure of bioactive alkaline-earth silicophosphate glasses. Mater Res Bull. 1994;29:1297–306. doi:10.1016/0025-5408(94)90154-6
36. Tatsumisago M, Kowada Y, Minami T. Raman spectra of rapidly quenched glasses and melts containing large amounts of Li_2O. J Non Cryst Solids. 1992;150:207–11. doi:10.1016/0022-3093(92)90124-3
37. Abd El-Moneim A. DTA and IR absorption spectra of vanadium tellurite glasses. Mater Chem Phys. 2002;73:318–22. doi:10.1016/S0254-0584(01)00355-8
38. Majjane A, Chahine A, Et-Tabirou M, Echchahed B, Do TO, Breen PM. X-ray photoelectron spectroscopy (XPS) and FTIR studies of vanadium barium phosphate glasses. Mater Chem Phys. 2014;143:779–87. doi:10.1016/j.matchemphys.2013.10.013
39. Karabulut M, Metwalli E, Brow RK. Structure and properties of lanthanum-aluminum-phosphate glasses. J Non Cryst Solids. 2001;283:211–9. doi:10.1016/S0022-3093(01)00420-3
40. Pires RA, Abrahams I, Nunes TG, Hawkes GE. The role of alumina in aluminoborosilicate glasses for use in glass-ionomer cements. J Mater Chem. 2009;19:3652–60. doi:10.1039/b822285a
41. Metwalli EE, Brow RK, Stover FS. Cation effects on anion distributions in aluminophosphate glasses. J Am Ceram Soc. 2001;84:1025–32. doi:10.1111/j.1151-2916.2001.tb00785.x
42. Abou Neel EA, Chrzanowski W, Pickup DM, O'Dell LA, Mordan NJ, Newport RJ, et al. Structure and properties of strontium-doped phosphate-based glasses. J R Soc Interface. 2009;6:435–46. doi:10.1098/rsif.2008.0348
43. Rao KJ, Sobha KC, Kumar S. Infrared and Raman spectroscopic studies of glasses with NASICON-type chemistry. Proc Indian Acad Sci Chem Sci. 2001;497–514. doi:10.1007/BF02708786
44. Dayanand C, Bhikshamaiah G, Java Tyagaraju V, Salagram M, Krishna Murthy ASR. Structural investigations of phosphate glasses: A detailed infrared study of the x(PbO)-(1-x)P_2O_5 vitreous system. J. Mater. Sci. 1996;1945–67. doi:10.1007/BF00356615
45. Tsai PP, Greenblatt M. Lithium ion conducting glasses in the system LiCl-Li_2O-P_2O_5-SiO_2. J Non Cryst Solids. 1988;103:101–7. doi:10.1016/0022-3093(88)90421-8
46. Saad M, Stambouli W, Sdiri N, Elhouichet H. Effect of mixed sodium and vanadium on the electric and dielectric properties of zinc phosphate glass. Mater Res Bull. 2017;89:224–31. doi:10.1016/j.materresbull.2017.01.043
47. Magdas DA, Vedeanu NS, Toloman D. Study on the effect of vanadium oxide in calcium phosphate glasses by Raman, IR and UV-vis spectroscopy. J Non Cryst Solids. 2015;428:151–5. doi:10.1016/j.jnoncrysol.2015.08.012
48. Marzouk MA, Elbatal FH, Abdelghany AM. Ultraviolet and infrared absorption spectra of Cr_2O_3 doped - sodium metaphosphate, lead metaphosphate and zinc metaphosphate glasses and effects of gamma irradiation: A comparative study. Spectrochim Acta - Part A Mol Biomol Spectrosc. 2013;114:658–67. doi:10.1016/j.saa.2013.05.093
49. Zachariasen WH. The atomic arrangement in glass. J Am Chem Soc. 1932;54:3841–51. doi:10.1021/ja01349a006